ACS APPLIED MATERIALS & INTERFACES

Research Article

www.acsami.org

Comparison of Electromagnetic Shielding with Polyaniline Nanopowders Produced in Solvent-Limited Conditions

Hesham Ramzy Tantawy,[†] D. Eric Aston,*[,†] Jacob R. Smith,[‡] and Jeffrey L. Young[‡]

[†]Department of Chemical and Materials Engineering and [‡]Department of Electrical and Computer Engineering, University of Idaho, 875 Perimeter Drive, MS 1021, Moscow, Idaho 83844-1021, United States

Supporting Information

ABSTRACT: Nanoparticle synthesis (~10−50 nm) of HCl-doped polyaniline elucidates the impact of limiting solvent (water) and oxidizing agent (ammonium peroxydisulfate) on morphology (XRD and TEM), chemical structure (FTIR), conductivity (two-point DC) and electromagnetic shielding effectiveness (SE) in microwave frequencies (i.e., X-band S-parameter measurements). Detailed comparison of these properties with respect to three distinct polymerization environments indicate that a solvent-free or limited solvent polymerization accomplished through a wet grinding solid-phase reaction produces superior conductivity (27 S/cm) with intermediate crystallinity (66%) for the highest EM shielding—an order of magnitude improvement over conventional polymerization with respect to EM power transmission reduction for all loadings per shielding area (0.04 to 0.17 g/cm^2). By contrast, the classic oxidation of aniline in a well-dispersed aqueous reaction phase with an abundance of available oxidant in free solution yielded low conductivity (3.3 S/cm), crystallinity (54%), and SE, whereas similar solvent-rich reactions with limiting oxidizer produced similar conductivity (2.9 S/cm) and significantly lower SE with the highest crystallinity (72%). This work is the first to demonstrate that limiting solvent and oxidizer enhances electromagnetic interactions for shielding microwaves in polyaniline nanopowders. This appears connected to having the highest overall extent of oxidation achieved in the wet solid-phase reaction.

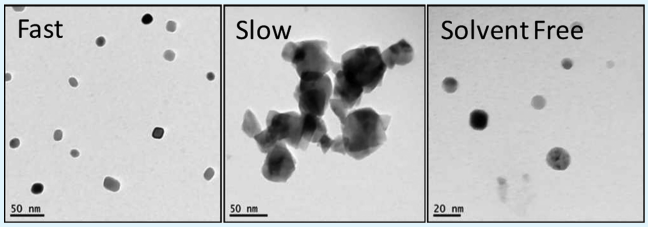

KEYWORDS: *polyaniline, solvent free, electromagnetic interference, shielding effectiveness, X-band*

1. INTRODUCTION

The proliferation of electronic devices in the world has caused electromagnetic interference (EMI) to become a vital concern. Although all electronics emit magnetic and electrical energy, if this energy unintentionally interacts with another device and causes it to malfunction, then it is considered interference.[1] In fact, EMI has become a serious dilemma impacting almost all contemporary electrical and electronic systems from daily life to space exploration.[2] A device is considered electromagnetically compatible—having low EMI with its surroundings—if it does not interfere with other devices or itself and it is not affected by emissions from other devices.[3] Therefore, good shielding materials should prevent both incoming and outgoing EMI. Its shielding effectiveness (SE), expressed in decibel (dB) units, is considered adequate for many applications at roughly 30 dB, corresponding to 99.9% attenuation of the EMI radiation.[4] The standard requirements for any application are specific to frequency range and geometry.

Various shielding methods have been developed not only to reduce the probability of EMI occurrence but also to increase device lifetime and efficiency.[1] Traditional approaches to EMI shielding rely on the use of metallic materials, which generally provide excellent SE. However, conventional metallic shields impose severe weight penalties, especially for aerospace applications.[5] Intrinsically conducting polymers (ICPs) are more attractive materials due to their lightweight, versatility, low cost, and processability.[6] ICPs have relatively high conductivities (σ) and dielectric constants (ε_r) that are easy to control or design through chemical processing.[7] Moreover, ICPs have significant EMI shielding through absorption that also improves shielding against potential internal EMI, which differs from the dominant metal and carbon-based shielding mechanism of reflection.[8] Among the host of ICPs is polyaniline (PANI), regarded as a promising conductive polymer because of superior conductivity control through doping with relatively easy polymerization of large quantities and its other electromagnetic parameters being flexibly adjustable through both oxidation and protonation states.[5,9,10]

Typically, PANI can be made chemically or electrochemically by oxidative polymerization of aniline.[11] Electrochemical methods have the merit of easier control over morphology and electrical properties but difficulty in mass production. Chemical methods are generally more effective for commercial-scale mass production.[12,13] The conventional chemical synthesis of PANI is based on mixing aniline with an oxidant in aqueous, or nonaqueous, acidic media.[10,14]

Received: October 1, 2012
Accepted: May 14, 2013
Published: May 14, 2013

Recently, attention has been paid to the preparation of doped-PANI via solvent-free reaction approaches accomplished in a solid state.[15−21] This has obvious advantages by eliminating the solvent costs and complications associated therein, including separation, recovery, reuse and proper waste treatment as well as reducing the overall volume and mass per final product quantity. Furthermore, a solvent-free reaction is the more environmentally benign method.[16] However, the EM properties of solvent-free PANI and their controllability remain largely unstudied, and the electromagnetic shielding potential of PANI nanoparticles or nanopowders synthesized by a solvent-free reaction is not evident in available literature.

The present study details the physicochemical characteristics of PANI doped with HCl synthesized via a wetted solid state polymerization under mechanical grinding, referred to as a "solvent-free" protocol (SF), compared with two conventional chemical approaches for both fast (CF) and slow (CS) oxidation conditions in aqueous solutions of ammonium peroxydisulfate (APS)—the same oxidizing agent used in the solvent-free route—evolving into lyophobic colloidal suspensions. After careful determination of chemical and morphological structures through analysis of Fourier transform-infrared (FTIR) spectra, X-ray diffraction (XRD), and transmission electron microscopy (TEM), the three nanopowders as compressed disks and annuli are tests for conductivity (DC) and electromagnetic wave propagation, respectively, in order to correlate nanomaterial properties with bulk behaviors relevant for EMI shielding. The first comparison of shielding effectiveness (SE) is made on a basis of mass loadings required per area of shielding material to be used within the microwave X-band frequency range (8−12 GHz) for the three conducting nanopowders. This type of synthetic, analytic, applications-oriented process sequence is crucial for the future advancement of affordable, lightweight EMI shielding formulations with these types of nanopowders as filler components in polymer or ceramic matrices, such as for coatings, films, sheets, and paints.

2. THEORY OF ELECTROMAGNETIC INTERFERENCE SHIELDING

Shielding effectiveness (SE) is the ratio of residual energy to impinging energy, usually equivalent to the total electromagnetic (EM) radiation transmitted (subscript T) through the shielding divided by the incident (subscript i) wave. This can be calculated from any of the energy intensities: electric (E), magnetic (H), electromagnetic power (P)[2,22]

$$SE = -20\log\left(\frac{E_T}{E_i}\right) = -20\log\left(\frac{H_T}{H_i}\right) = -10\log\left(\frac{P_T}{P_i}\right) \quad (1)$$

The EMI attenuation is dependent on frequency, distance between shield and interfering source, shield thickness, and of particular interest, shield material. SE is normally expressed in decibels (dB).[2]

There are three primary EM/material interaction mechanisms contributing to SE. Part of the incident radiation is reflected from the front surface of the shield, part is absorbed within the shield material, and part is reflected from the rear surface to the front, where it can either aid or hinder the effectiveness of the shield depending on its phase relationship with the incident wave, as shown in Figure 1. Therefore, the total effectiveness of a shielding material (SE_{Total}) equals the sum of the absorption losses (SE_A), the reflection losses (SE_R),

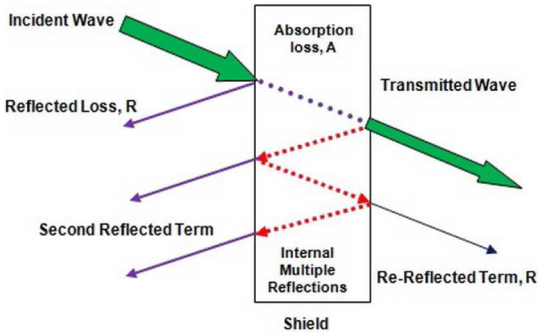

Figure 1. Attenuation schematic of an electromagnetic wave by shielding material.

and a correction factor (M) to account for multiple reflections, which may be significant in thin shields[23]

$$SE_{total} = SE_A + SE_R + M \quad (2)$$

The multiple reflection factor M is usually neglected where the absorption loss is greater than 10 dB. For simplified calculations, it may be neglected for electric fields and plane waves. Furthermore, absorption losses are a function of the physical characteristics of the shield and are independent of source field type.[2] The absorption, or decay, loss occurs because currents induced in the medium produce ohmic losses and heating of the material.[1] On the other hand, the reflection loss is related to the relative mismatch between the incident wave and the surface impedance of the shield. Moreover, multiple reflection correction factors can be mathematically positive or negative (in practice, it is always negative) and become insignificant when $SE_A > 6$ dB. It is usually only important at low frequencies (i.e., below approximately 20 kHz)[2] after therefore of insignificant impact to the present study concerning the microwave X-band.

In a two-port network analysis, EMI SE can be expressed in terms of scattering parameters that quantify the way currents and voltages travel in a transmission line when encountering a discontinuity caused by differing impedances between air and the obstruction or in the dielectric media.[24] In a waveguide, a radiated wave undergoes shielding (reflection, absorption, and transmission) when the incident wave at a point i passes toward another point j, and these wave scattering values are expressed as S_{ji}. For example, S_{21} is the energy acquisition at point 2 having originated from point 1 Therefore, the scattering parameters S_{11} and S_{21} designate the amount of reflected energy and transmitted energy, respectively. To investigate the contributions of absorption and reflection to the total EMI SE, the transmittance (T_{coef}), reflectance (R_{coef}), and absorbance (A_{coef}) coefficients can be correlated to S parameters as follows[25]

$$T_{coef} = [E_T/E_i]^2 = {S_{12}}^2 = {S_{21}}^2 \quad (3)$$

$$R_{coef} = [E_R/E_i]^2 = {S_{11}}^2 = {S_{22}}^2 \quad (4)$$

$$A_{coef} = 1 - T_{coef} - R_{coef} \quad (5)$$

Here, the term A_{coef} is given with respect to the power of the incident EM wave. If the effect of multiple reflections between both interfaces of the material is negligible,[26] the relative intensity of the effectively incident EM wave inside the shielding layer after reflection is based on the value of (1 −

R_{coef}). Therefore, the effective absorbance can be described as follows

$$A_{eff} = \frac{1 - T_{coef} - R_{coef}}{1 - R_{coef}} \quad (6)$$

Hence, by applying the power balance data, SE_R and SE_A can be expressed in terms of transmittance and reflectance, respectively[27]

$$SE_R = 10\log(1 - R_{coef}) \quad (7)$$

$$SE_A = 10\log(1 - A_{coef}) = 10\log\left(\frac{T_{coef}}{1 - R_{coef}}\right) \quad (8)$$

$$\therefore SE_T = 10\log\left(\frac{T_{coef}}{1 - R_{coef}}\right) + 10\log(1 - R_{coef}) \quad (9)$$

3. MATERIALS AND METHODS

Batches of HCl-doped polyaniline nanoparticles were produced from three different synthesis protocols to make approximately 5 g of recovered product per batch using aniline (99.5%, ACS reagent grade, Aldrich) purified by distillation with zinc dust before use.[28,29] The inorganic acid dopant hydrochloric acid (37.43%, ACS reagent grade, EMD Chemicals) and the oxidant ammonium peroxydisulfate (98%, ACS reagent grade, Aldrich) were used as received. Ammonium peroxydisulfate (APS) was selected from a wide array of potential chemical oxidants based on a summative assessment of the relevant literature indicating generally higher polymer conductivities from APS than others, in conjunction with being a common and affordable chemical.

HCl-doped polyaniline (PANI) nanoparticle samples were prepared by solvent-free (SF) and conventional (solvent-based) chemical oxidations under slow (CS) and fast (CF) production rates as controlled by the addition of aqueous ammonium peroxydisulfate (APS), both described below in detail. All reaction protocols are designed for an targeted 50% level of dopant, which is expected to maximize conductivity in the products, where amine site protonation occurs above 50% and imine sites deprotonate below 50%.[12] However, the precise level of doping achieved is not easily determined and may be an additional source of uncertainty in interpreting physicochemical behavior. Because all three protocols involve the same constituents, only varying the methods of mixing, an operating hypothesis for similar chemical mechanism(s) producing systematically different product yields is reasonable. In the solvent-free extreme case, local reactant concentrations are maximized, compared to the much more dilute and uniform reaction conditions of the two conventional processes.

Polyaniline doped with HCl is reported to be quite stable regarding thermal and environmental stability.[15,16,22] It should be noted for safety precautions that benzidine is a well-known carcinogen and intermediate product of the electrochemical mechanism for preparing polyaniline, though it is highly susceptible to copolymerization and does not persist in detectible amounts under final reaction conditions with APS. This is perhaps an important, secondary motivation for avoiding electrochemical methods to alleviate any environmental and health concerns; however, this topic deserves continued awareness and vigilance in the laboratory, for waste management, and potential future technology developments.

3.1. Solvent-Free (SF) Synthesis. It should be first noted that the "solvent-free" label refers to the aniline monomer and oxidant (APS) being used in their as-prepared and as-received states without first dissolving them in a reaction medium (solvent), though certainly the SF reaction chemicals are not completely void of solvent since the dopant (HCl) is applied from the standard aqueous concentrate. A typical solvent-free polymerization procedure at room temperature (~18−24 °C) was followed with freshly distilled aniline (0.05 mol per batch) poured into a porcelain mortar, and then 0.1 mol of the doping acid, i.e., concentrated HCl was added dropwise while grinding manually for 10 min. The acid was added in very small dropwise portions in order to minimize the released fumes and prevent the overheating of the reaction medium since aniline reacts violently with strong acids.[30] The reactant mixture became a white paste after grinding.

Separate grinding of 0.05 mol of APS in another porcelain mortar produced a fine powder, which was subsequently added in small portions to the white paste reactant in order to avoid overheating from the highly exothermic oxidative polymerization.[31,32] Approximately 0.5 g of APS was added in between grinding the reactant mixture for ~1−2 min in cycles until the entire batch was uniformly ground and finally attained the appropriate dark green color indicative of the HCl-doped PANI nanoparticles. This product was transferred to a 2 L beaker where 100 mL of acetone, 100 mL of ethanol, and 800 mL of DI were added then mixed for 1 h in order to quench the polymerization reaction and to dissolve oligomeric impurities.[33−35] An excess volume of water was used to ensure a thorough washing for materials analysis.

A 5 μL sample of the mixture was taken and diluted with 10 mL of ethanol for morphological characterization. The rest of the product mixture was filtered and washed with acetone, ethanol, and distilled water, in series, until the initially brown filtrate became colorless in order to confirm the adequate removal of unreacted chemicals and excess acid.[36,37] Less than 500 mL of DI water was typically required for washing. A slower soaking process produced similar results with only 100 mL of acetone, 200 mL of ethanol, and 100 mL of DI water. It is likely that ethanol and acetone requirements may be further reduced through future optimizations for practical materials applications for combined quenching and washing. The powder was dried at 40 °C for 48 h.

Although typical molecular weights for polyaniline prepared by chemical oxidation can be expected of 30 000 g/mol,[38] it will be very important for future work to consider a comparative molecular-weight distribution study of the solvent-free products against the conventional products of the present study.

3.2. Conventional Chemical Synthesis: Fast (CF) and Slow (CS) Oxidations. The same freshly distilled aniline in 0.05-mol doses was dissolved in 1000 mL of DI water followed by dropwise addition of 0.1 mol of HCl concentrate with mixing on a magnetic stirrer (1000 rpm) for 15 min. Then 0.05 mol of APS dissolved in 50 mL of DI was added. In case of conventional chemical oxidation with fast reaction (CF), the oxidizing APS solution was added all at once. On the other hand, the slow reaction procedure (CS) added the same APS solution amount with constant rate 0.1 mL/min. Both reaction protocols were conducted at room temperature (~18−24 °C). The reaction mixtures were mixed for 12 h after APS addition. Then 100 mL of acetone and 100 mL of ethanol were added and mixed for 1 h, similar to the SF samples above except that no additional DI water is needed for the conventional solvent-rich synthesis.[33−35] As before, 5 μL samples of these mixtures were also taken and diluted with 10 mL of ethanol for comparative morphological characterizations with the SF samples. The remaining products were filtered, washed, and dried identically to the SF samples. However, it must be noted that these conventional chemical synthesis products required in excess of three liters of DI water per batch to wash at the same level of filtrate clarity as the solvent-free product, as well as 500 mL of ethanol and 300 mL of acetone with clear room for process optimization.

4. CHARACTERIZATION METHODS

4.1. Chemical: FTIR. The doped PANI samples as dry powders were characterized for chemical constituencies with a ThermoNicolet Avatar 370 FTIR spectrometer equipped with an attenuated total reflectance (ATR) attachment. The 16 spectra for each sample type were collected between 1800 cm^{-1} and 650 cm^{-1} at a resolution of 4.0 cm^{-1} and averaged.

4.2. Morphological: TEM. Morphological characterization was carried out by transmission electron microscopy (TEM-JEOL JEM 2010) operating 200 kV. A drop of diluted suspension of each sample was applied to a copper grid coated with carbon film (FCF-150-Cu).

4.3. Crystallinity: XRD. A Siemens D5000 powder X-ray diffractometer was used for XRD characterization using a copper target (Cu Kα) and wavelength (λ) of 0.15418 nm. Data were collected in the range of $2\theta = 10-60°$ at a resolution of 0.02° per step with a 1 s integration time per step. The crystallinity of the PANI nanostructures were calculated by "DIFFRACplus EVA" software and obtained as the crystalline area divided by the sum of crystalline and amorphous areas.[34]

The *d*-spacings were deduced from the angular position (2θ) of the observed peaks according to the Bragg formula:[39] $\lambda = 2d\sin\theta$. The crystalline domain size, or the extent of order L, of the highest intensity crystallite peak was estimated using the Scherrer formula:[34] $L = k\lambda/(\beta\cos\theta)$, where k is the shape factor for the average crystallite (≈ 0.9), and β is the peak's full width at half-maximum (fwhm) in radians.[40] The interchain separation length (R), corresponding to the most intense crystallite peak of Bragg diffraction patterns from the PANI samples, was determined from the relation given by Klug and Alexander:[41] $R = 5\lambda/(8\sin\theta)$.

4.4. Electrical Conductivity. Electrical conductivity of the samples was measured at room temperature on pressed pellets by a two-point probe technique.[17,42,43] Typically, 0.1 g samples were pelletized at 70 MPa for 3 min using a hydraulic press.[44] The obtained pellet dimensions were 13-mm diameter and 1-mm thickness. Three pellets were prepared for each sample. Current–voltage ($I-V$) measurements were carried out via a Keithley 4200 SCS semiconductor parameter analyzer. Dual sweep mode was operated within a voltage range −1 to 1 V, and 0.01 V stepwise. Five physical locations were measured on each pellet side to confirm consistency within each sample: one location at the center of the pellet and four others nearer the edge in the four adjacent quadrants. Each $I-V$ measurement was repeated five times at least for every location for reproducibility confirmation. The values reported are averaged over 25 readings for each sample.

4.5. Electromagnetic Shielding. Electromagnetic shielding measurements used an Agilent E8363A PNA vector network analyzer in the X-band (8.2–12.4 GHz). Two open-ended waveguides filled with Teflon at the waveguide end and the sample holder were employed (Figure 2).[45] The dimension of the cross-section of the waveguide and the sample holder is 22.86 mm × 10.16 mm.[23] The length of the sample holder is 7 mm. The sample holder was filled with the PANI nanoparticle samples of known masses to specified depths by manual compaction for consistent density between replicates with excellent reproducibility due to careful measurements described below. No matrix material was added. The holder is inserted into the two waveguides; see the Supporting Information for photographs of the waveguide sample holder.

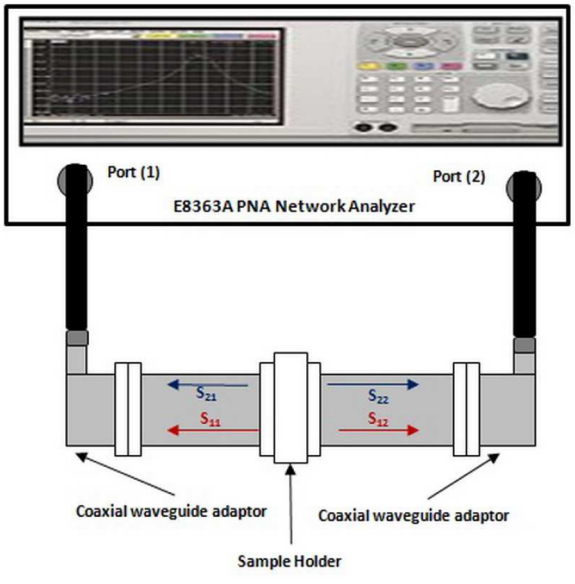

Figure 2. EMI waveguide measurement setup.

To quantify the S-parameter accurately using the vector network analyzer, the measurement system was calibrated by the Thru–Reflect–Line (TRL) calibration.[23,45] To investigate the EM shielding potential of the HCl-doped PANI nanopowders prepared from different synthetic approaches, seven different mass loadings of each sample type were used: 0.1, 0.15, 0.2, 0.25, 0.3, 0.35, and 0.4 g, corresponding to sample areal concentrations, or areal densities, of 0.04, 0.06, 0.09, 0.11, 0.13, 0.15, and 0.17 g/cm^2, respectively. This notation was selected to provide a more direct standard for mass loading comparisons with SE trends, since SE is proportional to the shield thickness and areal density factors out the thickness. The 0.1 g samples were compacted to 1.6 mm sample thickness for the conventional nanopowders (CF and CS) and 0.9 mm for the solvent-free product. Each additional 0.05 g of nanoparticles increased the sample thicknesses by 0.8 mm and 0.5 mm, respectively. Compacting depth was measured to within ±0.05 mm. Each sample was tested for the SE_T of the HCl-doped PANI at different mass loadings as a function of frequency measured in the 8–12 GHz range for the purpose of discussing the dependence of SE_T on absorption and reflection losses and the EM shielding potential as a function of the areal concentration with respect to the synthesis conditions.

5. RESULTS AND DISCUSSION

5.1. Morphology. TEM micrographs show that fast oxidation of HCl-doped PANI nanoparticles (PANI-HCl-CF) leads to the formation of very regular nanopolygons as well as some irregular spherical nanoparticles (Figure 3a). The average

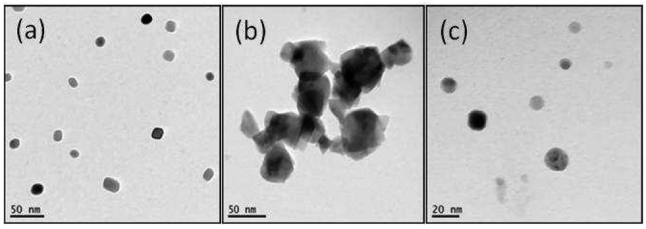

Figure 3. TEM images of HCl-doped polyaniline: (a) fast oxidation, (b) slow oxidation, (c) solvent-free formulation. Note scale bars of 50 nm in a and b but 20 nm for c.

particle size is less than 50 nm. There is an obvious contrast with the slow oxidation products (PANI-HCl-CS) giving much larger aggregates with more irregularities to the nanopolygon morphologies and a broad particle size distribution. The largest primary particles typically observed for both CF and CS samples generally do not exceed 50 nm with many more fused clusters in the CS samples. The solvent-free samples (PANI-HCl-SF) consisted of regular nanopolygons and nanospheres with an estimated particle size of 20 nm and less (note the smaller scale in Figure 3c from the CF and CS micrographs). It is intriguing that previous studies on solvent-free and solid-state synthesis approaches reported nanofibers rather than the nanoparticles produced in this work.[15,18]

5.2. Current–Voltage ($I-V$) Characterization. The current–voltage ($I-V$) curves of the HCl-doped PANI samples are shown in Figure 4, indicating ohmic behavior in all types at room temperature.[46] All sample types behaved as perfect ohmic conductors with the electrical resistance increasing as follows: SF < CF < CS. The highest conductivity was for SF (27.19 ± 0.26 S/cm) followed by CF (3.28 ± 0.25 S/cm) with CS (2.94 ± 0.14 S/cm) slightly lower. The differences are of course due to the impact of the formulation conditions on the final chemical structure and material crystallinity, which will be

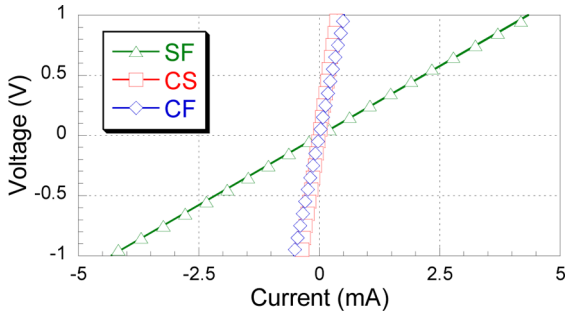

Figure 4. *I*–*V* curves from two-point probe measurements on three polyaniline sample types doped with HCl.

discussed later. The experimental values of conventional HCl-doped PANI (CF and CS) fitted within in the range of conductivities previously reported for PANI.[32] However, the nearly order of magnitude increase in conductivity for the SF samples is higher than recently reported.[16,17,21]

5.3. Fourier Transform Infrared (FTIR) Spectroscopy Analysis. Representative FTIR spectra of the PANI samples prepared (SF, CF, and CS), are shown in Figure 5. The positions of the bands differ only within experimental error from the positions measured by others.[47−50] These previous interpretations of PANI spectra together with corresponding references are summarized in Table 1 and associated with the three sample types studied herein.

FTIR spectra are characterized by two major regions I and II. Region I (1100−1700 cm^{-1}), in which the C−C and C−N stretching and C−H bending are expected of molecules containing aromatic rings.[49] The pair of bands near 1580 cm^{-1} and 1490 cm^{-1} are attributed to C═C stretching of quinonoid (N═Q═N) and benzenoid (N═B═N) ring-stretching vibrations, respectively.[47,51] Moreover, C−N bending vibration modes are observed near 1295 cm^{-1} for aromatic amines.[49,52] Furthermore, the bands characteristic of conducting protonated PANI are found at ∼1245 cm^{-1}, which corresponds to (C−N^{+}•) stretching vibration in the polaron structure.[47]

The broad band centered at 1148 cm^{-1} has been assigned to the vibration mode of the −NH^{+}= structure and is associated with the vibrations of the charged polymer units Q═NH^{+}−B or B−NH^{+}•−B and/or to the aromatic hydrocarbon (C−H) in-plane deformation.[53] The absorption band increases with increasing degree of protonation in the PANI backbone. This band has been related to the high degree of electron delocalization in PANI as well as to strong interchain (NH^{+}−N) hydrogen bonding.[47,54] The peak located near 1040 cm^{-1} suggests the presence of sulfonate or bisulfate groups, possibly from the oxidizing agent, attached to the aromatic rings.[47,50,53,55] Alternately, it could be attributes to C−H in-plane bending.[49,50,56]

The PANI-HCl-CS spectrum has two absorption bands of particular interest. The first at 1445 cm^{-1}, which is attributed to the skeletal (C═C) stretching vibration of substituted aromatic rings,[47,50,53] supports the presence of ortho-coupled and phenazine-like units.[55,65] The second is a weak band at 1375 cm^{-1}, which is characteristic of standard PANI base material (i.e., undoped) and assigned to C−N stretching in the vicinity of a quinonoid ring,[55,66] also an indication of the existence of phenazine-like structures.[47,65]

Region II (<1100 cm^{-1}), which corresponds to ring deformation,[57] contains the modes related to ring deformations with select C−H out-of-plane vibrations.[49] The observed band near 820 cm^{-1} is due to the C−H out-of-plane bending vibrations of two adjacent hydrogen atoms on a 1,4-disubstituted benzene ring.[47,49,58] This confirms the dominant para-coupling of constitutional units in the PANI chains. In particular, the PANI-HCl-CS spectrum shows significant amounts of 1,2,4-trisubstituted benzene ring, appearing in bands at 881 and 862 cm^{-1} indicative of the formation of branched and/or substituted phenazine-like segments[53,67] in addition to absorption band at 796 cm^{-1}, which is attributed to C−H out-of-plane bending vibrations of 1,2-disubstituted benzene ring.[47,50]

Based on the previous data in which the quinonoid and benzenoid units were identified, the intensity ratio of these two absorption bands around 1580 cm^{-1} and 1490 cm^{-1} is indicative of the average extent of the oxidation state of the polymer, which reflects the content of the quinoid and benzene ring structures.[57] The intensity ratio *R* is calculated as $I_{quinoid}$ over $I_{benzenoid}$. Table 2 shows that the ordering of *R* values is SF

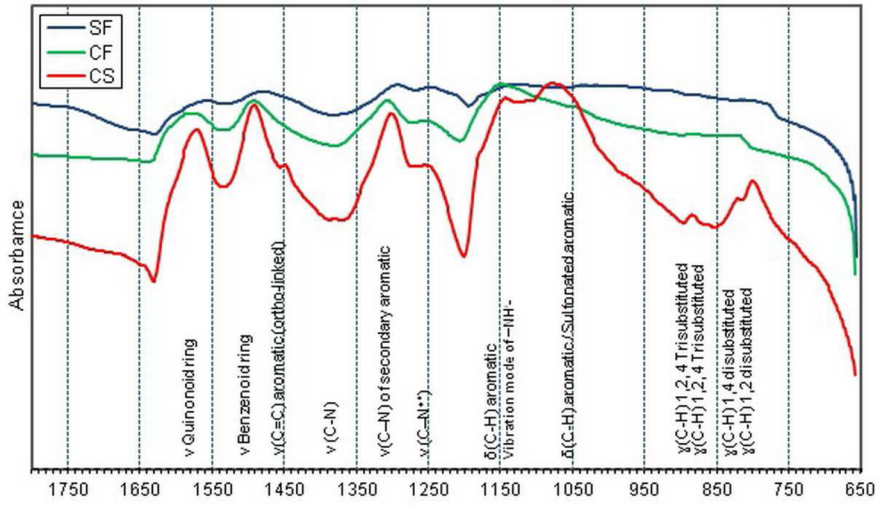

Figure 5. FTIR spectra (in wavenumbers of cm^{-1}) of HCl-doped polyaniline prepared with different synthesis conditions: SF (top), CF (middle), CS (bottom).

Table 1. The main IR bands for PANI-HCl nanoparticles by synthesis condition

	wavenumber (cm^{-1})				
no.	SF	CF	CS	assignment	ref
1			797	C−H out-of-plane ring bending 1,2-disubstituted	47,50
2	815	823	819	C−H out-of-plane ring bending (1,4 disubstituted ring)	47,49,57,58
3			862	C−H out-of-plane ring bending (1,2, 4 trisubstituted ring)	51,54,59,60
4			881	C−H out-of-plane ring bending (1,2, 4 trisubstituted ring)	51,54,59,60
5	1035	1043	1077	C−H in plane bending	49,50,56
				sulfonated aromatic ring (HSO_4^-/SO_2^-)	47,50,53,55
6	1121	1147	1140	C−H in plane bending	53,61,62
				vibration mode of $-NH^+-$	
7	1240	1248	1248	C−N stretching ($C-N^+\bullet$)	47,54
8	1290	1302	1298	C−N stretching secondary aromatic amine	47,54,63
9			1375	C−N stretching (Q═N−B)	47,55,61
10			1445	C═C aromatic ring or N═N Stretching	47
				C═C aromatic ring (ortho-linked)	55,64,65
11	1479	1487	1489	benzenoid (B) ring-stretching	17,32,47,61,65
12	1556	1580	1588	quinonoid (Q) ring-stretching	17,32,47,61,65

Table 2. Absorption Intensities and Their Ratios for PANI-HCl Samples

synthesis method	$I_{quinoid}$	$I_{benzenoid}$	R
CF	0.922	0.957	0.963
CS	0.885	0.948	0.934
SF	0. 955	0.980	0.974

> CF > CS. The results suggest that there is a difference in the extent of oxidation state of the prepared samples depending on the synthesis approach, since the reactants and oxidizer ratios are fixed. The relatively lower oxidation extent in the CS samples could be attributed to its structure, which according to the previous interpretation supports the suggestion of increase in nonlinear chains due to the presence of cross-linking structures from coupling in the ortho- position.[64,65] The CS approach may be favorable for cross-linking and branched PANI allowed by the slower oxidation, which means PANI chains growing with other existing chains, with higher probability of structural defects impacting the electrical and electronic behavior.[58,65]

5.4. XRD Characterization. Even though all the three PANI sample types are doped with HCl for the same chemical composition, the XRD patterns show distinct differences between each as shown clearly in Figure 6. The similarity between the XRD patterns of the SF and CS samples is relatively clear with sharper peaks compare to the fast oxidation product (CF), which confirms the presence of high crystallinity and/or ordering in the samples with significant rate-limiting conditions imposed on their reactions. In order to visualize the peaks better and separate the contributions of different crystalline and amorphous constituencies in the XRD pattern, Figures 6b−d employ a single-line method using Voigt function.[68,69] The results agree with what has been mentioned in the literature; within 2θ from 10 to 60°, that the three main diffraction peaks of emeraldine salt were resolved. In addition, two weak peaks rise at approximately 27 and 29°, seen in

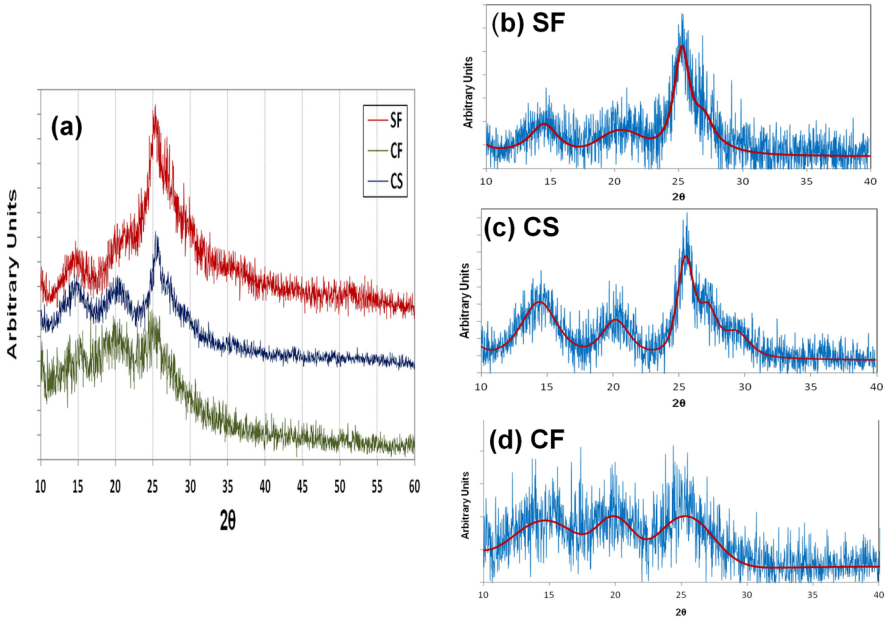

Figure 6. XRD patterns of HCl-doped polyaniline nanoparticles from different syntheses.

Table 3. XRD Data Analysis Summary

sample	2θ	d (Å)	domain size L(Å)	interchain separation (Å)	(hkl)	crystallinity (%)
PANI-HCl-CF	13.90	6.36			(010)	53.8 ± 0.3
	19.67	4.51			(100)	
	24.36	3.65	46.33 ± 8.12	4.51	(011)	
PANI-HCl-CS	14.54	6.09			(010)	73.2 ± 2.9
	19.70	4.51			(100)	
	25.60	3.48	132.32 ± 9.02	4.34	(011)	
PANI-HCl-SF	14.64	6.05			(010)	65.9 ± 2.1
	20.94	4.24			(100)	
	25.24	3.53	121.63 ± 9.09	4.41	(011)	

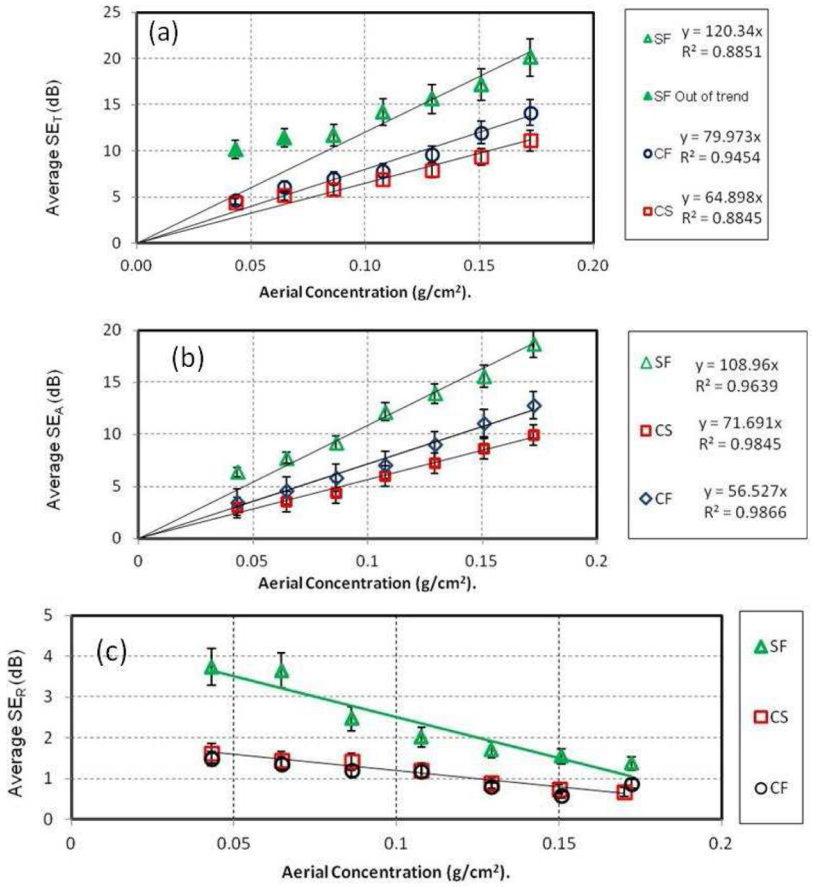

Figure 7. Shielding effectiveness (SE) averaged over the tested X-band range of 8−12 GHz: (a) total (SE_T), (b) absorbance component (SE_A), and (c) reflectance component (SE_R), identifying linear trends for CF, CS, and SF type HCl-doped PANI nanopowders. Error bars represent standard deviations.

PANI-HCl-CS (Figure 6c). The observed *d*-spacing of the Bragg reflections are compatible with orthorhombic lattice symmetry.[17,64,70]

Crystalline peaks can be observed near 15 and 25°, which correspond to the (010) and (110) planes of crystalline PANI domains, respectively (Table 3). An amorphous peak can be seen at 20° that corresponds to the (100) plane[36] and also represents the characteristic distance between the ring planes of benzene in adjacent chains or the close-contact interchain distance,[16] while the peaks at 2θ = 25° may be caused by periodicity perpendicular to the polymer chain. The percentages of crystallinity for each sample type are approximately 54, 73, and 66% corresponding to CF, CS, and SF, respectively. The obtained results were the average of three or more XRD measurements. Both SF and CS samples are significantly more crystalline than the CF material.

The high crystallinity of CS could be due to the formation of cross-linking structures from coupling in the ortho- position[64] encouraged by the slow oxidation conditions. In addition, slow exothermic polymerization with no noticeable change in the temperature of the reaction medium is a favorable condition for higher degree of crystallinity[65] compared to CF and SF. The reason that the SF nanoparticles have higher crystallinity than CF is perhaps due to the formation of its chains under relatively concentrated acidic condition,[17] though it may be difficult to reconcile this with the slow oxidation process at lower local acid concentrations producing the highest crystallinity. Apparently, both slow oxidation and high acidity favor high crystallinity in

dx.doi.org/10.1021/am401695p | ACS Appl. Mater. Interfaces 2013, 5, 4648−4658

HCl-doped PANI, supporting the general notion that the degree of crystallinity depends on the synthesis approach.[64]

CF and SF samples consist mainly of linear chains as it was explained from the FTIR discussion. The conventional trends between crystallinity, d−spacing, interchain separation, crystalline domain size, and conductivity are clearly observed.[71] The SF samples exhibit larger domain size, shorter d−spacing and interchain separation, and higher conductivity than the fast oxidation (CF) product, as might also be expected by differences in linear polymer chain density. The regularity and organized structure defined by crystallinity is a favorable factor mainly for intramolecular mobility of charged species along the chain and to some extent intermolecular hopping because of better and/or closer packing.[71] For this reason, SF nanoparticle samples are roughly ten times more conductive than CF samples. There is, of course, a difficulty in reconciling the highest crystallinity of the three formulations being found for CS samples with the lowest conductivity.

In the particular case of the slow oxidation product, the highly crystalline materials is cross-linked and/or branched more than the other two types, resulting from a shorter conjugated length and localized polarons for a lower conductivity.[58] A further interpretive complication arises from the crystalline domain sizes for CF and CS samples being smaller than the particle sizes observed with the TEM. This suggests that rather than a blend two populations of fully crystalline and fully amophorous PANI nanoparticles, it is more likely that most nanoparticles have an internal blend of crystalline, transition, and amorphous regions.[72] Without knowing the quantitative characteristics in this regard from the analytical techniques and quality available for this work, these variations in nanoparticle morphology could easily account for the relativity lower conductivity of CF and CS sample types with respect to the SF nanopowder. On the other hand, the obtained crystalline domain sizes for SF HCl-doped PANI were very close to the estimated particle size observed with TEM, which may be an indication of the presence of nearly single-crystal nanoparticles. It may be deduced that the SF approach allows the proper ordering and oxidation extent of PANI molecules and contributes to the higher conductivity than the HCl-doped PANI samples prepared with the classical chemical oxidation approaches (CF and CS).

5.5. Electromagnetic (EM) Measurements. The application of PANI-based nanomaterials in EM shielding manufacturing will be as a filler in some convenient matrix, or perhaps on its own if appropriate forming conditions can be achieved to preserve, or even enhance, final product SE. Therefore, it is important to relate its shielding effectiveness behaviors with the employed amount per unit surface area, also called areal concentration (mass/area). Figure 7a−c compiles the average values for SE_T, SE_A, and SE_R of the all doped PANI sample types and loadings as function of the areal concentrations, showing roughly linear behavior in shielding, with two distinct outliers for the solvent-free samples at the lowest mass loadings. As expected, the total shielding efficiency (SE_T) increased with increasing the mass loaded in the sample holder of each sample type (CF, CS, SF). Figure 7a shows SE_T for PANI samples as a function of EM frequency in the X-band for each mass loading, as well as the absorbance and reflection curves (Figure 7b-c). By increasing the amount of nanopowder loaded from 0.1 to 0.4 g, the average SE_T roughly triples from 5 to 14 dB for CF samples. With a constant cross-section, this effect is due to the shielding material thickness increasing,[5,7] where the EM wave power traveling through a medium should decay exponentially.[67]

SE_T increased slightly with higher frequencies. This behavior is likely associated with the existence of two types of charged species in doped PANI: (1) polaron/bipolaron systems that are mobile along the chain and 2) other bound charge distributions (e.g., dipoles) with restricted mobility accounting for strong polarization in the system.[12,73] When the frequency of the applied field is increased, the dipoles cannot reorient as rapidly as the applied electric field. This decreases the dielectric constant and increases the number of mobile charges, which results in higher dielectric loss (ε''), whereas the real part (ε') decreases.[26,74,75] The product of angular frequency (ω) and dielectric loss is equivalent to the dielectric conductivity (σ_{ac}, microwave ac conductivity) as follows[75,76]

$$\sigma_{ac}(\omega) = \omega\varepsilon'' = \omega\varepsilon_o\varepsilon''_r = 2\pi f\varepsilon_o\varepsilon''_r \quad (10)$$

where ε_o is the free space permittivity, ε''_r is relative dielectric loss of the medium, and f is the frequency. Higher dielectric loss leads to increasing microwave ac conductivity and the effective conductivity of the medium:[77−79] $\sigma_e(\omega) = \sigma_{dc}(\omega) + \sigma_{ac}(\omega)$. This may explain the aforementioned enhancement in SE_T by increasing the frequency. In the microwave region, σ_{ac} of emeraldine salts is larger than σ_{dc}, though still near the same order of magnitude.[74,80] For this reason, σ_{dc} of PANI still has a significant impact on the SE.

The similarly increasing trends for SE_A with mass loading (Figure 7b) show that the absorption mechanism dominates the total shielding and increases from 75 to 90% of the total contribution, whereas SE_R shows limited impact, decreasing with mass loading from 1.5 to 0.9 dB (Figure 7c) for both CF and CS samples. The SE_A contributions for CS are lower (67−89% for 0.1−0.4 g, respectively) than found for the CF HCl-doped PANI nanopowders. This could be attributed to an increasing reflection coefficient with sample thickness[81,82] or an impedance mismatch between the incident wave impedance (377 Ω) and the surface impedance expected when dealing with conductive PANI samples.[2] A decreasing trend with frequency has previously been attributed to the decreasing surface impedance with thicker samples.[83,84]

The results for HCl-doped PANI nanoparticles show an interesting contradiction to the general rule that higher crystallinity should increase conductivity,[44,70,85−87] whereas the CS PANI nanopowders are significantly more crystalline (Table 3) with arguably similar or lower conductivity and slightly lower shielding than CF PANI samples. If high crystallinity were achieved with the formation of cross-linking structures due to coupling in the ortho- position, the proton mobility is expected to be lower than that in linear doped PANI samples in which head-to-tail (i.e., N-para) coupling is predominant.[64] The proposed cross-linking structures in CS samples may arise from the slow oxidation of aniline by restrictive reagent addition (APS solution at 0.1 mL/min ≈ 0.11 mol/min), which fosters PANI chain growth with existing chains as well as other structural defects resulting in lower conductivity.[58,65] Moreover, the slow polymerization produces no noticeable change in temperature of the reacting mixture, which is favorable for higher degrees of crystallinity.[65] Because both fast and slow oxidation products (CF and CS) were synthesized with the same dopant (HCl) ratios, the degree of crystallinity appears to depend only on the reaction conditions[64] and thus an optimum in conductivity and crystallinity for the maximum shielding potential may be

revealed with fine-tuning of the rate and method for oxidant addition.

The solvent-free (SF) HCl-doped PANI nanopowders were the most successful of the three products in shielding the X-band frequencies (Figure 7). Similar trends in SE_T and SE_A with mass loading follow the results for the conventional products; however, the SE was much greater overall, mostly due to the much higher conductivity. Figure 7a indicates significantly greater increases in SE_T for the lower mass loadings over both CF and CS sample types. Figure 7b indicates that relative absorption effects (SE_A is 63−93% of shielding from 0.1 to 0.4 g) are smallest for SF PANI samples at the lower loadings but match and slightly exceed relative contributions in the other two sample sets. Therefore, the contribution of SE_R again decreases with mass loading (Figure 7c) but is also greater in magnitude for each case compared to the conventional products (3.7 to 1.4 dB with increasing mass loads). Clearly, conductivity and not crystallinity is the direct controlling factor herein for the most favorable EM shielding, where losses occur as a result of ohmic current induced in the shield and dissipated as heat; therefore, the magnitude of the EM losses depends on the shield thickness and conductivity.[5,22,88]

It is noteworthy that although both absorption and reflection terms exhibit fairly strong linear correlations, especially for the conventional oxidation products, the SE_T data trends arguably show some biexponential character, viz., upward curvature, across all three nanoparticle formulations. This would seem to support the need for deeper understanding into the function form of the multiple reflection term, M, according to shield thickness, which was earlier dismissed as negligible. The linear trends in SE_T and SE_A for increasing areal concentrations generally agree with the fact that the attenuation of the propagating EM wave exponential.[2,89] However, the decreasing trend in average SE_R, attributed to increasing surface impedance as the thickness increases, currently lacks a clear functional-form connection; that is, no single phenomenological factor appears to suggest an explanation for an apparent exponential decrease in reflective shielding effectiveness due to path length.

6. CONCLUSIONS

The main contribution of this work is highlighting the dependence of EM shielding effectiveness (SE) in conducting polymers on the synthesis approach, particularly in the microwave X-band for polyaniline nanopowders doped with HCl. The solution-free or solvent-limited synthesis in a slightly wetted solid-phase reaction provides substantial material property improvements over conventional solution-rich oxidations with limited or abundant oxidizer (CS and CF samples, respectively). Collective data analysis demonstrates the importance of conductivity over crystallinity for enhancing SE for nanoPANI. The synthesis protocols that lead to maximizing crystallinity (e.g., conventional slow oxidation) in HCl-doped PANI with cross-linked structures or branched chains is not recommended, as there appears to be an intermediate optimum with respect to conductivity and EM shielding.

The total shielding versus nanopowder loading curves exhibit slight but consistent deviations from the expected exponential decay behavior for EM wave propagation, indicative of a significant multiple reflection effect in the nanomaterials. Therefore, it is likely that even greater shielding may be achieved at higher loadings, with alterations in size distributions, and certainly with the addition of higher reflectance materials, such as metals, in a mixed nanocomposite with a PANI-containing matrix. The latter is a promising approach with potential trade-offs between materials cost and mass loading as well as an extra controllable parameter for flexibility in fabrication for specific EMI design criteria. In addition, a thin insulating nanoparticle coating, such as PANI without dopant, has the potential to produce higher surface impedance and lower reflection coefficient in the compacted nanopowder to increase SE_R. In parallel with these studies, the dopant species and level—held constant herein—may be optimized, as well.

■ ASSOCIATED CONTENT

Ⓢ Supporting Information

Photographs of the waveguide, X-band measurements, and original data of shielding effectiveness versus frequency for the X-band of all three polyaniline sample types. This material is available free of charge via the Internet at http://pubs.acs.org.

■ AUTHOR INFORMATION

Corresponding Author

*E-mail: aston@uidaho.edu.

Author Contributions

The manuscript was written through contributions of all authors. All authors have given approval to the final version of the manuscript.

Notes

The authors declare no competing financial interest.

■ ACKNOWLEDGMENTS

The authors gratefully acknowledge support for this research from the Military Technical College (Cairo, Egypt); professors Aicha Elshabini and Fred Barlow; and expert technical assistance and instrument access from Thomas J Williams (TEM, XRD), Charles Cornwall, and David MacPherson (EM shielding sample holder fabrication), and Professor Armando McDonald (FTIR).

■ REFERENCES

(1) Weston, D. A. *Electromagnetic Compatibility: Principles and Applications*; Marcel Dekker: New York, 2001.
(2) Tong, X. C. *Advanced Materials and Design for Electromagnetic Interference Shielding*; CRC Press: Boca Raton, FL, 2009.
(3) Paul, C. R. *Introduction to Electromagnetic Compatibility*; John Wiley & Sons: Hoboken, NJ, 2006.
(4) Li, L.; Chung, D. D. L. *Composites* **1991**, *22*, 211−218.
(5) Wang, Y.; Jing, X. *Polym. Adv. Technol.* **2005**, *16*, 344−351.
(6) Cao, G. *Nanostructures and Nanomaterials: Synthesis, Properties, and Applications*; Imperial College Press: London, 2004.
(7) Joo, J.; Epstein, A. J. *Appl. Phys. Lett.* **1994**, *65*, 2278−2280.
(8) Skotheim, T. A.; Reynolds, J. R. *Handbook of Conducting Polymers 2: Conjugated Polymers−Processing and Applications*. CRC Press: Boca Raton, FL, 2007.
(9) McManus, P. M.; Cushman, R. J.; Yang, S. C. *J. Phys. Chem.* **1987**, *91*, 744−747.
(10) Bhadra, S.; Khastgir, D.; Singha, N. K.; Lee, J. H. *Prog. Polym. Sci.* **2009**, *34*, 783−810.
(11) Wan, M. *Conducting Polymers with Micro or Nanometer Structure*; Tsinghua University Press: Beijing, 2008.
(12) Wallace, G. G.; Spinks, G. M.; Kane-Maguire, L. A. P.; Teasdale, P. R. *Conductive Electroactive Polymers Intelligent Materials Systems*; CRC Press: Boca Raton, FL, 2009.
(13) Toshima, N.; Hara, S. *Prog. Polym. Sci.* **1995**, *20*, 155−183.
(14) Han, M. G.; Cho, S. K.; Oh, S. G.; Im, S. S. *Synth. Met.* **2002**, *126*, 53−60.

(15) Zhou, C. F.; Du, X. S.; Mai, Y. W.; Liu, Z.; Ringer, S. P. *Synth. Met.* **2009**, *159*, 1302−1307.
(16) Bekri-Abbes, I.; Srasra, E. *J. Polym. Res.* **2011**, *18*, 659−665.
(17) Abdiryim, T.; Xiao-Gang, Z.; Jamal, R. *Mater. Chem. Phys.* **2005**, *90*, 367−372.
(18) Du, X. S.; Zhou, C. F.; Wang, G. T.; Mai, Y. W. *Chem. Mater.* **2008**, *20*, 3806−3808.
(19) Abdiryim, T.; Jamal, R.; Nurulla, I. *J. Appl. Polym. Sci.* **2007**, *105*, 576−584.
(20) Ding, Y.; Abdiryim, T.; An, S.; Nurulla, I. *J. Appl. Polym. Sci.* **2008**, *107*, 3864−3870.
(21) Huang, J.; Moore, J. A.; Acquaye, J. H.; Kaner, R. B. *Macromolecules* **2004**, *38*, 317−321.
(22) Nalwa, H. S. *Handbook of Organic Conductive Molecules and Polymers, Conductive Polymers: Spectroscopy and Physical Properties*; Wiley: Chichester, U.K., 1997; Vol. 3.
(23) Chen, L. F.; Ong, C. K.; Neo, C. P.; Varadan, V. V.; Varadan, V. K. *Microwave Electronics: Measurement and Materials Characterization*; John Wiley & Sons: Hoboken, NJ, 2004.
(24) Yun, J.; Im, J. S.; Lee, Y.-S.; Kim, H.-I. *Eur. Polym. J.* **2010**, *46*, 900−909.
(25) Klemperera, C. J. v.; Maharajb, D. *Compos. Struct.* **2009**, *91*, 467−472.
(26) Reddy, B. In *Advances in Nanocomposites−Synthesis, Characterization and Industrial Applications*; Reddy, B. S. R., Ed.; InTech: New York, 2011; pp 429−482.
(27) Al-Saleh, M. H.; Sundararaj, U. *Carbon* **2009**, *47*, 1738−1746.
(28) Chowdhury, P.; Saha, B. *Indian J. Chem. Technol.* **2005**, *12*, 671−675.
(29) Li, Y.; Al-Ghamdi, A. A.; Al-Hartomy, O. A.; El-Tantawy, F.; Yakuphanoglu, F. *Optoelectron. Adv. Mater., Rapid Commun.* **2012**, *6*, 235−238.
(30) Pohanish, R. P.; Greene, S. A. *Wiley Guide to Chemical Incompatibilities*, 3rd ed.; Wiley: Hoboken, NJ, 2009.
(31) Fu, Y.; Elsenbaumer, R. L. *Chem. Mater.* **1994**, *6*, 671−677.
(32) Stejskal, J.; Gilbert, R. G. *Pure Appl. Chem.* **2002**, *74*, 857.
(33) Nalwa, H. S. *Handbook of Organic Conductive Molecules and Polymers, Conductive Polymers: Synthesis and Electrical Properties*; Wiley: Chichester, U.K., 1997; Vol. 2.
(34) Bhadra, S.; Khastgir, D. *Polym. Test.* **2008**, *27*, 851−857.
(35) Zhang, X.; Zhu, J.; Haldolaarachchige, N.; Ryu, J.; Young, D. P.; Wei, S.; Guo, Z. *Polymer* **2012**, *53*, 2109−2120.
(36) Varma, S. J.; Xavier, F.; Jayalekshmi, S.; Varghese, S. *Polym. Int.* **2012**, *61*, 743−748.
(37) Majumdar, D.; Baskey, M.; Saha, S. K. *Macromol. Rapid Commun.* **2011**, *32*, 1277−83.
(38) Freund, M. S.; Deore, B. *Self-Doped Conducting Polymers*; John Wiley & Sons: Hoboken, NJ, 2007.
(39) Ladd, M. F. C.; Palmer, R. A. *Structure Determination by X-ray Crystallography*; Plenum Press: New York, 1994.
(40) Cullity, B. D. *Elements of X-ray Diffraction*; Addison-Wesley: Reading, MA, 1956.
(41) Klug, H. P.; Alexander, L. E. *X-Ray Diffraction Procedures for Polycrystalline and Amorphous Materials*; Wiley: New York, 1974.
(42) Rimbu, G. A.; Stamatin, I.; Jackson, C. L.; Scott, K. *J. Optoelectron. Adv. Mater.* **2006**, *8*, 670−674.
(43) Duan, Y.; Shunhua, L.; Hongtao, G. *Sci. Technol. Adv. Mater.* **2005**, *6*, 513−518.
(44) Zhang, D. *Polym. Test.* **2007**, *26*, 9−13.
(45) Ebara, H.; Inoue, T.; Hashimoto, O. *Sci. Technol. Adv. Mater.* **2006**, *7*, 77−83.
(46) Mzenda, V. M.; Goodman, S. A.; Auret, F. D. *Synth. Met.* **2002**, *127*, 285−289.
(47) Trchovâa, M.; Stejskal, J. *Pure Appl. Chem.* **2011**, *83*, 1801.
(48) Schrader, B. *Infrared and Raman Spectroscopy: Methods and Applications*; VCH: Weinheim, Germany, 1995.
(49) Boyer, M. I.; Quillard, S.; Rebourt, E.; Louarn, G.; Buisson, J. P.; Monkman, A.; Lefrant, S. *J. Phys. Chem. B* **1998**, *102*, 7382−7392.
(50) Socrates, G. *Infrared and Raman Characteristic Group Frequencies: Tables and Charts*; Wiley: Chichester, U.K., 2000.
(51) Kang, E. T.; Neoh, K. G.; Tan, K. L. *Prog. Polym. Sci.* **1998**, *23*, 277−324.
(52) Ameen, S.; Kim, Y. S.; Shin, H. S.; Akhtar, M. S. *Chem. Eng. J.* **2011**, *181−182*, 806−812.
(53) Stejskal, J.; Trchová, M. *Polym. Int.* **2012**, *61*, 240−251.
(54) Prokes, J.; Trchova, M.; Hlavata, D.; Stejskal, J. *Polym. Degrad. Stab.* **2002**, *78*, 393−401.
(55) Stejskal, J.; Trchova, M.; Konyushenko, E. N.; Sapurina, I. *Macromolecules* **2008**, *41*, 3530−3536.
(56) Stejskal, J.; Trchova, M.; Prokes, J.; Sapurina, I. *Chem. Mater.* **2001**, *13*, 4083.
(57) Quillard, S.; Louarn, G.; Lefrant, S.; Macdiarmid, A. G. *Phys. Rev. B* **1994**, *50*, 12496−12508.
(58) Pan, L. J.; Pu, L.; Shi, Y.; Sun, T.; Zhang, R.; Zheng, Y. O. *Adv. Funct. Mater.* **2006**, *16*, 1279−1288.
(59) Miller, F. A.; Mayo, D. W.; Hannah, R. W. *Course Notes on the Interpretation of Infrared and Raman Spectra*; Wiley-Interscience: Hoboken, NJ, 2004.
(60) Kellenberger, A.; Dmitrieva, E.; Dunsch, L. *J. Phys. Chem. B* **2012**, *116*, 4377−4385.
(61) Trchová, M.; Stejskal, J.; Prokeš, J. *Synth. Met.* **1999**, *101*, 840−841.
(62) Laslau, C.; Zujovic, Z.; Travas-Sejdic, J. *Prog. Polym. Sci.* **2010**, *35*, 1403−1419.
(63) Laska, J.; Widlarz, J. *Polymer* **2005**, *46*, 1485−1495.
(64) Liu, H.; Hu, X. B.; Wang, J. Y.; Boughton, R. I. *Macromolecules* **2002**, *35*, 9414.
(65) Stejskal, J.; Sapurina, I.; Trchova, M. *Prog. Polym. Sci.* **2010**, *35*, 1420−1481.
(66) Sedenková, I.; Trchová, M.; Stejskal, J.; Bok, J. *Appl. Spectrosc.* **2007**, *61*, 1153−62.
(67) Hayt, W. H.; Buck, J. A. *Engineering Electromagnetics*, 8th ed.; McGraw-Hill: London, 2012.
(68) Banerjee, S.; Saikia, J.; Kumar, A.; Konwar, B. *Nanotechnology* **2010**, *21*, 045101.
(69) Pramanik, S.; Karak, N.; Banerjee, S.; Kumar, A. *J. Appl. Polym. Sci.* **2012**, *26*, 830−836.
(70) Chaudhari, H. K.; Kelkar, D. S. *Polym. Int.* **1997**, *42*, 380−384.
(71) Sinha, S.; Bhadra, S.; Khastgir, D. *J. Appl. Polym. Sci.* **2009**, *112*, 3135−3140.
(72) Mazerolles, L.; Folch, S.; Colomban, P. *Macromolecules* **1999**, *32*, 8504−8508.
(73) Nalwa, H. S. *Advanced Functional Molecules and Polymers*; Gordon and Breach Science: Amsterdam, 2001.
(74) Chandrasekhar, P.; Naishadham, K. *Synth. Met.* **1999**, *105*, 115.
(75) Micheli, D.; Apollo, C.; Pastore, R.; Marchetti, M. *Compos. Sci. Technol.* **2010**, *70*, 400−409.
(76) Abkowitz, M. A.; Lakatos, A. I. *J. Chem. Phys.* **1972**, *57*, 5033−5036.
(77) John, H.; Thomas, R. M.; Jacob, J.; Mathew, K. T.; Joseph, R. *Polym. Compos.* **2007**, *28*, 588.
(78) John, H.; Thomas, R. M.; Mathew, K. T.; Joseph, R. *J. Appl. Polym. Sci.* **2004**, *92*, 592−598.
(79) Moore, J. C.; Fujita, S. *J. Geophys. Res.* **1993**, *98*, 9769−9780.
(80) Javadi, H.; Cromack, K.; MacDiarmid, A.; Epstein, A. *Phys. Rev. B* **1989**, *39*, 3579−3584.
(81) Latyshev, A. V.; Yushkanov, A. A. *J. Opt. Technol.* **2012**, *79*, 316−321.
(82) Rajagopalan, H.; Rahmat-Samii, Y. *IEEE Trans. Antennas Propag.* **2010**, *52*, 73−89.
(83) Avloni, J.; Ouyang, M.; Florio, L.; Henn, A.; Sparavigna, A. *J. Thermoplast. Compos. Mater.* **2007**, *20*, 241−254.
(84) Avloni, J.; Florio, L.; Henn, A. R.; Lau, R.; Ouyang, M.; Sparavigna, A. *J. Thermoplast. Compos. Mater.* **2007**, *20*, 241−254.
(85) Bohli, N.; Gmati, F.; Mohamed, A. B.; Vigneras, V.; Miane, J. L. *J. Phys. D: Appl. Phys.* **2009**, *42*, 205404.
(86) Chaudhari, H. K.; Kelkar, D. S. *J. Appl. Polym. Sci.* **1996**, *62*, 15.

(87) Zhang, K.; Li, Y. *Polym. Adv. Technol.* **2011**, *22*, 2084−2090.
(88) Geetha, S.; Rao, C. R. K.; Vijayan, M.; Trivedi, D. C.; Kumar, K. K. S. *J. Appl. Polym. Sci.* **2009**, *112*, 2073−2086.
(89) Pozar, D. M. *Microwave Engineering*; Wiley: New York, 1997.